Bragg Scattering from a Random Potential

Donghwan Kim[1] and Eric J. Heller[2,1,*]

[1]*Department of Chemistry and Chemical Biology, Harvard University, Cambridge, Massachusetts 02138, USA*
[2]*Department of Physics, Harvard University, Cambridge, Massachusetts 02138, USA*

A potential for propagation of a wave in two dimensions is constructed from a random superposition of plane waves around all propagation angles. Surprisingly, despite the lack of periodic structure, sharp Bragg diffraction of the wave is observed, analogous to a powder diffraction pattern. The scattering is partially resonant, so Fermi's golden rule does not apply. This phenomenon would be experimentally observable by sending an atomic beam into a chaotic cavity populated by a single mode laser.

Monochromatic light or matter waves entering a perfectly periodic medium show sharp Bragg scattering into specific angles. However, randomly disturbing the perfect lattice positions results in diffuse scattering between the Bragg peaks. As the dispersion increases, the diffuse scattering eventually dominates and finally the Bragg peaks vanish. The diffuse scattering is structured, revealing correlations in the medium. For example, for x-ray scattering in water [1,2] and the scattering of visible light in disordered packing of monodisperse polystyrene beads [3,4], the pair correlation function has a broad peak with a characteristic length scale, which in turn generates a broad peak in the structure function.

In the studies of disordered media, the Bragg peaks are associated with periodic structures [5,6]. It is not expected, however, that a random medium, with no perfect order on any scale, can generate sharp scattering angles, yet we report such a case here. For the potential we choose, the spatial autocorrelation function has broad peaks as the atom pair correlation function in water, but the scattering angle nonetheless is very sharp. This is startling; the scattering in the random potential defined below is like Bragg scattering in a periodic potential, rather than the scattering in a correlated liquid. The closest analog—though not a perfect one—is powder diffraction with many randomly oriented crystallites packed closely. The potential defined below has no such "crystallites," yet it has Bragg peaks. We explain this surprise by calculating scattering matrix elements, or, equivalently, by examining the Fourier components of the potential. However, the time evolution of the scattering is not compatible with Fermi's golden rule, as discussed below.

We consider the following form of random potential

$$V(\vec{r}; \{\phi_j\}) = \frac{A}{\sqrt{N}} \sum_{j=1}^{N} \cos(\vec{q}_j \cdot \vec{r} + \phi_j), \quad (1)$$

where A is a constant having the dimension of energy, N is the number of modes, $\vec{q}_j = |\vec{q}_j|(\hat{x} \cos \theta_j + \hat{y} \sin \theta_j)$ are wave vectors, and $\theta_j = 2\pi(j-1)/N$ are angles equally spaced over 2π. This is a superposition of N plane waves of an equal amplitude A each propagates in different directions with a wave number $|\vec{q}_j|$, an angle θ_j, and a random phase shift ϕ_j. It is not important that the angle be equally spaced, or the amplitudes be the same, as long as they are random.

For simplicity, we consider a random potential constructed by equal wave number $|\vec{q}_j| = q$ (see Supplemental Material [7] for more general potentials). We call this a "Berry potential," a function introduced in connection with wave chaos [8,9]. This random potential is experimentally realizable in a laser cavity with a single mode laser (need not be single) with rough or ballistically chaotic walls, so that the wave inside is a random superposition of waves traveling in all directions.

In the limit of many modes $N \to \infty$, the spatial autocorrelation of the potential is (see Supplemental Material [7])

$$C(\delta\vec{r}) = \langle V(\vec{r})V(\vec{r} + \delta\vec{r}) \rangle = \frac{A^2}{2} J_0(q\delta r),$$

where J_0 is the zeroth-order Bessel function of the first kind. From the autocorrelation, we can obtain the root-mean-square of the potential

$$V_{\rm rms} = \sqrt{\langle (V(\vec{r}))^2 \rangle} = \sqrt{C(0)} = A/\sqrt{2}.$$

We study the dynamics of wave packets with an initial average momentum $\hbar k$ in the Berry potential $V(\vec{r})$ employing the second order split operator method [10]. To have a "weak" disorder strength, set the constant A such that the fluctuation of the potential $V_{\rm rms}$ is far smaller than the average kinetic energy of the wave $\langle T \rangle = (\hbar^2 k^2/2m)$, i.e.,
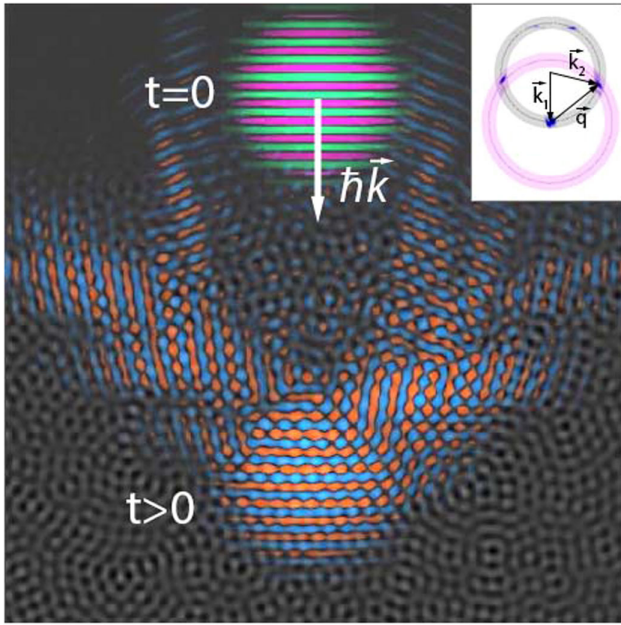
FIG. 1. Bragg scattering of a wave packet in a random (Berry) potential. The potential is drawn in gray scale on the background. An initial wave packet on the top launched downward into the potential with an average momentum $\hbar\vec{k}$ is depicted in green and magenta scale. The wave function at a later time is shown in red and blue scale. The inset shows the probability density of the wave at a later time in the reciprocal space in dark blue scale.

$V_{\mathrm{rms}} \ll \langle T \rangle$. Consideration of strong disorder strength $V_{\mathrm{rms}} \gtrsim \langle T \rangle$ is for future study [11].

Figure 1 shows the propagation of a wave packet in the Berry potential. The potential is drawn in gray scale on the background. There is a flat zero potential on the top and the Berry potential is smoothly turned on toward the bottom. An initial wave packet on the top launched downward into the potential with an average momentum $\hbar\vec{k}$ is depicted in green and magenta scale. The wave function at a later time is shown in red and blue scale. The wave is scattered by the random potential, initially only to the Bragg angle, but this is soon scattered again with the same Bragg angle relative to the motion, and so on. This scattering should not be confused with the higher order Bragg scattering that is absent if the Berry potential is composed only of sinusoids. The higher order scattering would be allowed if instead triangular waves were used, for example.

The inset in Fig. 1 shows the probability density of the wave at a later time in the reciprocal space in blue scale. The initial $\vec{k}_1$, final $\vec{k}_2$, and scattering $\vec{q}$ wave vectors are shown as in Ewald sphere construction [12,13]. For a given initial wave vector $\vec{k}_1$, the contour of equal energy can be drawn as a black circle. In addition, taking $\vec{k}_1$ as an origin, the nonzero Fourier components of the potential can be drawn as a magenta circle. Then, the Bragg scattered states appear at the intersections of the black and magenta circles [14]. It is seen that the scattered waves are populated only at

a Bragg angle. In three dimensions, the construction involves the intersection of spheres and thus the outgoing wave vectors $\vec{k}_2$ will lie on a ring corresponding to a Bragg angle.

The Bragg scattering of the wave in the Berry potential can roughly be interpreted as a superposition of the scattered waves by each constituent sinusoidal potential aligned in different directions. The situation is analogous to powder x-ray diffraction in which crystallites are aligned in all possible orientations, leading to the incoherent superposition of the outgoing waves from scattering by the crystallites. The conventional picture is that the scattering by some of the crystallites oriented properly with respect to incident x-ray beam leads to Bragg scattering, although this view has been challenged [15] in ways that are relevant to our present observations. Again there are no crystallites here, but the Berry potential bears some relation to the impossible limit of overlapping and blending them. In three dimensions, the scattered waves from the Berry potential will form a ring as is the case in the powder diffraction.

Employing the analogy above, by treating the wavelength $2\pi/q$ of the single sinusoid in the Berry potential as a "lattice spacing," one can write down the Bragg condition $n(2\pi/k) = 2(2\pi/q)\sin\theta$, which correctly explains our simulation result. Note only the first order ($n = 1$) Bragg angle θ_B satisfying $(2\pi/k) = 2(2\pi/q)\sin\theta_B$ is observed. Higher order ($n = 2, 3, \ldots$) Bragg angles will be observed if triangular, instead of sinusoidal, waves are used. Nevertheless, this analogy is not perfect since, in the random Berry potential, the superposition of the scattered waves by each sinusoidal component is coherent, rather than incoherent, which was the case in the powder diffraction as the phases of scattered waves from one crystallite to another do not match. The Berry potential coherence effect is manifested in the rapid growth of the scattered wave population as discussed below.

Consider scattering matrix element $\langle \vec{k}_2 | V | \vec{k}_1 \rangle \sim V_{\vec{k}_2 - \vec{k}_1}$, where $| \vec{k}_1 \rangle$ and $| \vec{k}_2 \rangle$ are plane wave states and $V_{\vec{k}_2 - \vec{k}_1}$ is the Fourier component of the potential. For elastic scattering ($|\vec{k}_1| = |\vec{k}_2| = k$), the scattering wave vector $\vec{q} = \vec{k}_2 - \vec{k}_1$ and scattering angle 2θ satisfy $q = 2k\sin\theta$, which coincide with the Bragg condition $n(2\pi/k) = 2(2\pi/q)\sin\theta$ for $n = 1$. Thus, allowed elastic scattering can actually be interpreted as Bragg scattering by a plane wave "lattice" of one sinusoidal component of the potential properly aligned with respect to the incident beam direction. The random Berry "medium" has no special directions of travel; all are equivalent and subject to Bragg diffraction at *relative* angle θ.

The scattering behavior of the wave varies considerably depending on its wavelength $2\pi/k$ compared to the wavelength of the sinusoids $2\pi/q$ used in the Berry potential. To understand the effect of length scales, we compare wave scattering for different values of reduced Planck's constant
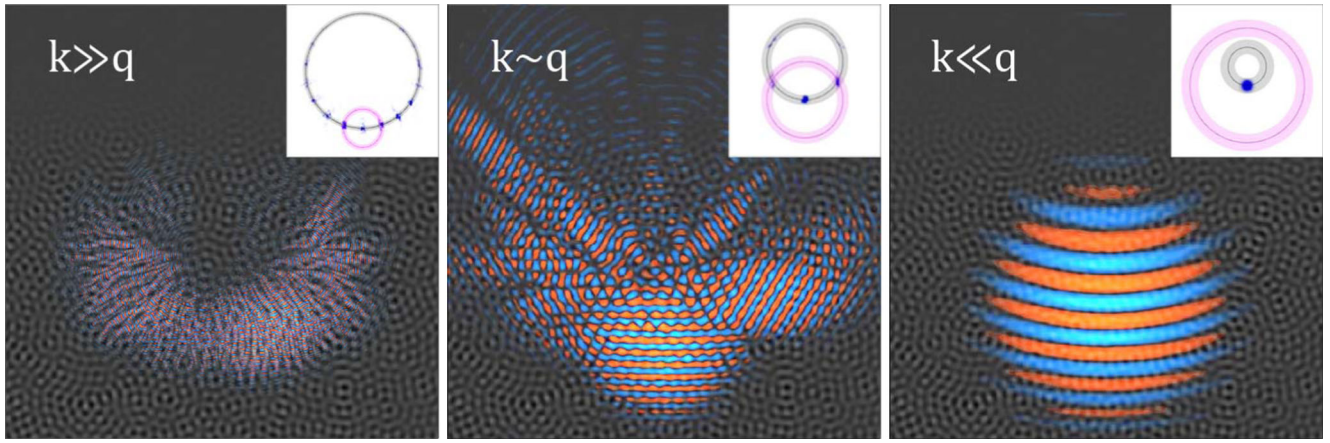
FIG. 2. Dependence of the wave evolution on $\hbar$. The real part of the wave function is plotted in red and blue scale and an inset in each panel shows the probability density distribution in the reciprocal space. For small $\hbar$, i.e., $k \gg q$ (small wavelength and classical limit), the wave dynamics is particlelike, diffusive, showing branched flow [16]. This is consistent with a very small Bragg angle which leads to repeated almost-forward scattering. For intermediate $\hbar$, i.e., $k \sim q$ the Bragg angle is not small, giving less classical-like diffractive behavior. For large $\hbar$, i.e., $k \ll q$ the wave is in a transparency regime: the wavelength is large enough that the small scale fluctuations of the potential are averaged to zero. Or equivalently, in reciprocal space, there are no intersections between the energy contour and the nonzero Fourier components of the potential. Therefore, there is effectively no scattering, and the potential is transparent.

$\hbar$, keeping the average momentum of the wave $\hbar k$ fixed. By keeping the momentum the same, the wave propagation speed and kinetic energy are kept the same for different $\hbar$'s, so the only physical difference comes from different wavelengths.

Depending on the value of $\hbar$ (so the wavelength), the wave packet scattering exhibits qualitatively different behaviors as shown in Fig. 2. For small $\hbar$, i.e., $k \gg q$ (small wavelength and classical limit), the wave dynamics is particlelike, diffusive, showing branched flow [16]. This is consistent with a very small Bragg angle which leads to almost-forward scattering. For intermediate $\hbar$, i.e., $k \sim q$ the Bragg angle cannot be treated to be small which results in less classical looking and diffractive behavior. For large $\hbar$, i.e., $k \ll q$ the wave is in a transparency regime; the wavelength is large enough that the smaller scale fluctuations of the potential are averaged to zero. Equivalently, in reciprocal space, there are no intersections between the energy contour and the nonzero Fourier components of the potential. Therefore, there is effectively no scattering, and the potential is transparent.

The first-order time-dependent perturbation theory gives the first-order correction to the wave function [17]

$$\psi^{(1)}(\vec{r}, t) = \int_0^t \phi(\vec{r}, t') dt', \qquad (2)$$

where the instantaneous scattered amplitudes $\phi(\vec{r}, t') = (1/i\hbar)e^{-iT(t-t')/\hbar}V(\vec{r})e^{-iTt'/\hbar}\psi(\vec{r}, 0)$ at different times t' interfere to form $\psi^{(1)}(\vec{r}, t)$. Figure 3 shows the first-order wave function $\psi^{(1)}(\vec{r}, t)$ from the wave packet initially launched downward. One can see the interference pattern formed by the superposition of $\phi(\vec{r}, t')$ at different times t'.

Also, the first-order wave function $\psi^{(1)}(\vec{r}, t)$ depends on the size and shape of the initial wave function $\psi(\vec{r}, 0)$ and the region of the potential the wave is spatially lying on. The asymmetry of the scattered waves shown in Figs. 1–3 is due to the asymmetry of the region of the potential right underneath the wave. This is not captured by the usual plane wave perturbation theory which predicts the symmetry of the scattered waves.
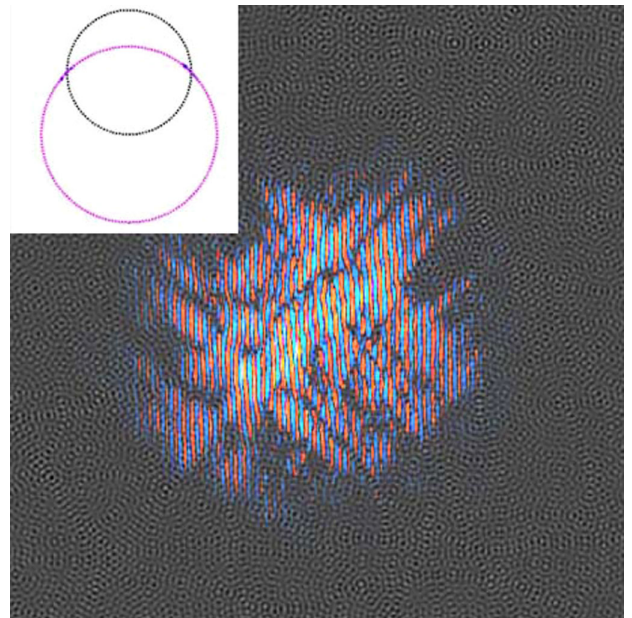

FIG. 3. The real part of the first-order wave function $\psi^{(1)}(\vec{r}, t)$ from a wave packet initially launched downward, showing the interference of the instantaneous scattered amplitudes from different times.
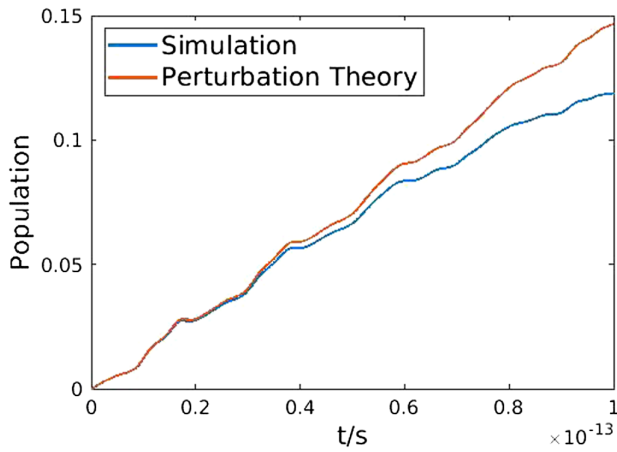
FIG. 4. Population of the scattered waves as a function of time. Blue and red curves correspond to simulation and first order time-dependent perturbation theory results, respectively. The population growth is not linear, i.e., Fermi's golden rule is not valid. Also, the population growth stops occasionally, showing that the pulses (scattered waves) come out sporadically as shown in Figs. 1 and 2. The two results coincide at early times when single scattering dominates. The discrepancy later is due to multiple scattering, absent in the first order time-dependent perturbation theory.

One can calculate the population $\langle \psi^{(1)}(t)|\psi^{(1)}(t)\rangle$ of the scattered waves from the first-order perturbation theory. The populations near the Bragg angle θ_B (so the scattering angle $2\theta_B$) were calculated in the simulation and compared with the perturbation theory as shown in Fig. 4. The nonlinear population growth indicates the breakdown of Fermi's golden rule. This behavior combines aspects of both resonant and nonresonant decay, which depends on the specifics of the interference of the scattered amplitudes $\phi(\vec{r}, t')$ in space and time [17]. Furthermore, the sometimes strong and irregular population growth oscillations are captured in the first-order time-dependent perturbation theory, explaining the sporadic pulses (scattered wave) coming out as shown in Figs. 1 and 2. Again, the plane wave perturbation theory does not correctly predict the population growth.

It is worth emphasizing the explanations given are not restricted to the two dimensional Berry potential, but are valid for more complicated forms of random potentials and in three dimensions as well. We checked the validity for more general two dimensional random potentials where the wave numbers $|\vec{q}_j|$ of the modes are different and even forming a "band" in reciprocal space (see Supplemental Material [7]). Also, as the explanations do not employ any specific property of two-dimensionality, they are expected to be valid in three dimensions as well.

Interestingly, there exists a momentum localization for special Bragg angles as shown in Fig. 5. A snapshot of the wave is shown after long propagation of a plane wave launched downward, in a 90° scattering (45° Bragg angle) situation. Of course, the scattered wings again rescatter at
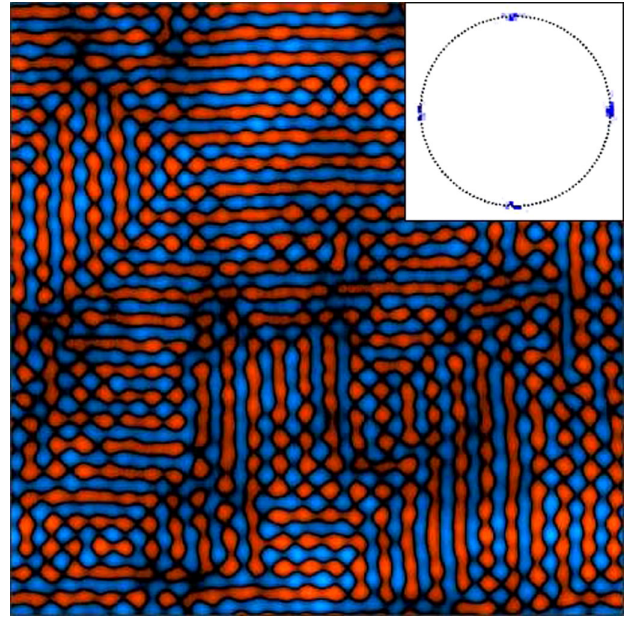

FIG. 5. Bragg scattering in a Berry potential: a special case of the 90° scattering angle. The real part of the wave function was plotted in red and blue scale. The inset shows the momentum space probability distribution of the wave. This is a snapshot, after a long time propagation of a downward launched wave packet. It is not diffusing in angle beyond the 90° turns, in spite of the random nature of the potential. A periodic boundary condition is used.

90°, and so on. There may result a permanent localization only to vertical and horizontal motion.

If the diffraction angle is $2\pi/N$ where N is a positive integer, the scattered wave comes back to the original incident angle after N scatterings, so the momentum distribution does not fill in the whole range of 2π. The special angles show localization of the wave in momentum space, assuming the initial wave packet is narrow enough in momentum space. In three dimensions, the situation is a little bit different from two dimensions, and the momentum localization will be possible only for scattering angle π [18].

We would like to emphasize that the presented results apply to any linear wave transport: not only to matter waves, but also to acoustic and electromagnetic waves.

The Berry potential may be used as a diffraction grating in the diffractive regime. If the incident beam is white, after passing the Berry potential, it will be broken into its constituent colors since different colors have different Bragg angles. The difference between the usual diffraction gratings and the Berry potential is that the diffraction pattern from the latter will be independent of the incident beam directions since the Berry potential is isotropically random.

In conclusion, although a random (Berry) potential lacks periodicity, sharp Bragg diffraction of the wave is observed in the potential, analogous to a powder diffraction pattern. Fermi's golden rule breaks down since the scattering is partially resonant. This phenomenon would be

experimentally realizable by sending an atomic beam into a chaotic cavity populated by a single mode laser.

MATLAB codes implementing the split operator method can be found in Ref. [19].

---

[*]eheller@fas.harvard.edu

[1] A. H. Narten, M. D. Danford, and H. A. Levy, X-ray diffraction study of liquid water in the temperature range 4200c, Discuss. Faraday Soc. **43**, 97 (1967).

[2] A. H. Narten and H. A. Levy, Liquid water: Molecular correlation functions from x-ray diffraction, J. Chem. Phys. **55**, 2263 (1971).

[3] S. K. Saini and R. V. Nair, Selective-frequency-gap-induced negative anisotropic scattering in designer photonic structures with short-range order, Phys. Rev. A **102**, 033529 (2020).

[4] V. Hwang, A. B. Stephenson, S. Magkiriadou, J.-G. Park, and V. N. Manoharan, Effects of multiple scattering on angle-independent structural color in disordered colloidal materials, Phys. Rev. E **101**, 012614 (2020).

[5] M. Rechtsman, A. Szameit, F. Dreisow, M. Heinrich, R. Keil, S. Nolte, and M. Segev, Amorphous Photonic Lattices: Band Gaps, Effective Mass, and Suppressed Transport, Phys. Rev. Lett. **106**, 193904 (2011).

[6] L. S. Froufe-Prez, M. Engel, J. J. Senz, and F. Scheffold, Band gap formation and anderson localization in disordered photonic materials with structural correlations, Proc. Natl. Acad. Sci. U.S.A. **114**, 9570 (2017).

[7] See Supplemental Material at http://link.aps.org/supplemental/10.1103/PhysRevLett.128.200402 for more general potentials.

[8] M. V. Berry, Regular and irregular semiclassical wavefunctions, J. Phys. A **10**, 2083 (1977).

[9] M. S. Longuet-Higgins, The statistical analysis of a random, moving surface, Phil. Trans. R. Soc. A **249**, 321 (1957).

[10] A. D. Bandrauk and H. Shen, Higher order exponential split operator method for solving time-dependent Schrödinger equations, Can. J. Chem. **70**, 555 (1992).

[11] The sum of the Berry potential considering thermal population leads to a deformation potential where we studied localization. See, D. Kim, A. Aydin, A. Daza, K. N. Avanaki, J. Keski-Rahkonen, and E. J. Heller, Coherent electron dynamics in thermal lattice vibrations (2022), arXiv:2005.14239.

[12] P. Ewald, Introduction to the dynamical theory of x-ray diffraction, Acta Crystallogr. Sect. A **25**, 103 (1969).

[13] N. Ashcroft and N. Mermin, *Solid State Physics*, HRW international editions (Holt, Rinehart and Winston, 1976).

[14] As the initial wave function has the momentum spread, $\vec{k}_1$ can be chosen to be any wave vector near the initial average value $\vec{k}$. The shaded gray and magenta area are the area covered by the collection of the black and magenta circles, respectively, considering all of the initial wave vector $\vec{k}_1$'s near the average value $\vec{k}$.

[15] P. F. Fewster, A new theory for x-ray diffraction, Acta Crystallogr. Sect. A **70**, 257282 (2014).

[16] M. A. Topinka, B. J. LeRoy, R. M. Westervelt, S. E. Shaw, R. Fleischmann, E. J. Heller, K. D. Maranowski, and A. C. Gossard, Coherent branched flow in a two-dimensional electron gas, Nature (London) **410**, 183 (2001).

[17] E. Heller, *The Semiclassical Way to Dynamics and Spectroscopy* (Princeton University Press, Princeton, NJ, 2018).

[18] In three dimensions, the scattering angle of $\pi/2$ will first fill the great circle of the equal energy sphere in reciprocal space. Then, the scattered waves on the great circle will be scattered again to fill the whole sphere, losing the localization feature. This is why only scattering angle of π will lead to localization in the reciprocal space in three dimensions.

[19] https://gitlab.com/public-codes/bragg-scattering-from-a-random-potential.

Correction: The affiliations were not presented properly owing to a conversion error and have been set right.